This is the peer-reviewed, final accepted version for American Mineralogist, published by the Mineralogical Society of America.
The published version is subject to change. Cite as Authors (Year) Title. American Mineralogist, in press.
DOI: https://doi.org/10.2138/am-2021-7731. http://www.minsocam.org/

REVISION R

THERMOELASTIC PROPERTIES OF ZIRCON: IMPLICATIONS FOR GEOTHERMOBAROMETRY

Alix M. Ehlers[1], Gabriele Zaffiro[2], Ross J. Angel[3*], Tiziana Boffa-Ballaran[4], Michael A. Carpenter[5], Matteo Alvaro[2], Nancy L. Ross[1]

[1]*Department of Geosciences, Virginia Polytechnic Institute and State University, Blacksburg, VA 24061, USA*
[2]*Department of Earth and Environmental Sciences, University of Pavia, Via A. Ferrata, 1 27100 Pavia, Italy*
[3]*IGG CNR, Via Giovanni Gradenigo, 6, 35131 Padova, Italy*
[4]*Bayerisches Geoinstitut, Universität Bayreuth Universitätsstraße 30, 95447 Bayreuth, Germany*
[5]*Department of Earth Sciences, University of Cambridge, Downing St, Cambridge CB2 3EQ, United Kingdom*

*Corresponding author: rossjohnangel@gmail.com

Submitted to: American Mineralogist

Date: 16-November-2020

ABSTRACT

A thermal-pressure equation of state has been determined for zircon ($ZrSiO_4$) that characterizes its thermoelastic behavior at metamorphic conditions. New pressure-volume (*P*-*V*) data from a "Mud-Tank" zircon have been collected from 1 bar to 8.47(1) GPa using X-ray diffraction, and elastic moduli were measured from room temperature up to 1172 K by resonance ultrasound spectroscopy. These data were fitted simultaneously with temperature-volume (*T*-*V*) data from the literature in EosFit7c using a new scaling technique. The parameters of a third order Birch-Murnaghan EoS with a Mie-Grüneisen-Debye model for thermal pressure has compressional EoS parameters K_{0T} = 224.5(1.2) GPa, K_{0T}' = 4.90(31) with a fixed initial unit-cell volume V_0 = 39.26 cm^3/mol and thermal parameters γ_0 = 0.868(15), q = 2.37(80), and Θ_D = 848(38) K. EoS parameters that describe the variation of unit-cell parameters with pressure and temperature were determined using an isothermal-type EoS. This new EoS confirms that zircons are stiffer than garnets and exhibit a much lower thermal expansion. This results in steep isomekes between

zircon and garnets, which makes zircon trapped as inclusions in garnets at metamorphic conditions a good piezothermometer.

INTRODUCTION

Zircon ($ZrSiO_4$) is an important and widespread mineral in the Earth's crust and upper mantle, commonly used to date geologic events using the U-Th-Pb geochronometer (e.g., Hanchar and Hoskin 2003). Because it is highly refractory, zircon is a common detrital component in many sedimentary deposits (e.g., Fedo et al. 2003) and can also be found as an accessory mineral in sedimentary, metamorphic, and igneous rocks (e.g., Finch and Hanchar 2003). Zircon can also be produced during prograde metamorphism as a result of the breakdown of minerals bearing Zr as a minor or trace component. It is therefore common for zircon crystals to be found trapped as inclusions, frequently within garnet hosts, as a result of garnet growth during prograde metamorphism. Zircon inclusions in garnet therefore have the potential to be used in piezobarometry in which the residual stress or pressure in the inclusions, arising from the contrast in the elastic properties of garnet and zircon, can be used to infer entrapment conditions (e.g., Angel et al. 2015). A reliable equation of state (EoS) for zircon is required for these calculations. However, zircon EoS parameters are poorly constrained. Reported isothermal bulk modulus values at room conditions vary substantially between K_{0T} = 198 GPa (Ono et al. 2004) and 227 GPa (Hazen and Finger 1979). A redetermination of the *P-V-T* EoS of zircon from the data available in the literature yields K_{0T} = 233 GPa and a pressure derivative of the bulk modulus of K_{0T}' = -0.56 (Zaffiro 2019), while the most recent ab-initio calculations report K_{0T}' = 4.71 (Stangarone et al. 2019).

In this paper, we present new data to resolve discrepancies between reported zircon EoS and determine a reliable thermal-pressure EoS. *P-V* data were measured using single-crystal X-ray diffraction, and values of the adiabatic bulk modulus, K_S, were obtained from the elastic tensor of a non-metamict zircon at high temperatures determined using resonant ultrasound spectroscopy (RUS). A Mie-Grüneisen-Debye (MGD) thermal-pressure EoS was determined from this new data plus literature data using a new scaling method in the fitting to remove bias and ensure consistency. The moduli values determined from the fitting and discussed in this paper are Reuss bound values, appropriate for describing the properties of zircon under

hydrostatic pressure. In this paper, we show that not only does our thermal-pressure EoS for zircon fit these data well, but the isobaric heat capacity C_p calculated from our EoS closely matches the experimentally-determined C_p values from the literature.

EXPERIMENTAL METHODS

P-V study

A portion of the standard sample UWZ-1, originating from the Mud Tank carbonatite complex near Alice Springs, Australia, was kindly provided by John Valley (University of Wisconsin). This sample is characterized by very low U/Th substitution and low amorphization, and has an estimated age of 732 Ma (e.g., Jackson et al. 2004; Yuan et al. 2018). Samples from the UWZ-1 bulk crystal were optically colorless which indicated low trace element abundances and low $^{176}Hf/^{177}Hf$ isotope ratios (Woodhead and Hergt 2005; Gain et al. 2019). SEM imaging, SIMS analyses of δO^{18} and OH/O, and δO^{18} laser fluorination measurements on the UWZ-1 sample by John Valley (pers. comm.) are consistent with chemical homogeneity.

Single-crystal X-ray diffraction experiments were conducted to determine the isothermal equation of state of Mud-Tank zircon. A single crystal of dimensions 160 μm x 110 μm x 40 μm was cut from this sample and loaded into an ETH-type diamond-anvil cell (Miletich et al. 2000) along with a single crystal of quartz as a pressure calibrant (Scheidl et al. 2016). Room-pressure unit-cell parameters were collected at 296 K, after which a pressure medium of 4:1 methanol:ethanol solution was loaded into the diamond-anvil cell and the cell was increased to higher pressures. Unit-cell parameters were collected using a Huber four-circle X-ray diffractometer with MoKα radiation, run by SINGLE software (Angel and Finger 2011). Unit-cell parameters of zircon were determined based on the 8-position centering method (King and Finger 1979) using 8-9 reflections, with $12.45 \leq 2\theta \leq 28.03$. In total, 18 measurements were collected in increasing pressure increments from 1 bar to 8.47(1) GPa. Three additional data points collected upon decompression of the cell were consistent within uncertainties with those collected upon compression (Table **1**).

RUS measurements

A second sample of the Mud-Tank zircon, sourced independently from a mineral dealer, was prepared in the form of a rectangular parallelepiped with polished faces parallel to (100), (010) and (001) within 0.5° as determined by X-ray diffraction measurements. It had dimensions of 4.637 x 4.628 x 3.166 mm^3 and a mass of 0.3167 g, which corresponds to a density of 4.661 g/cm^3, in comparison with a theoretical density calculated from the measured lattice parameters of 4.663 g/cm^3. There were chips out of the edges of the crystal but the fraction of the total volume and mass of the sample that these represented was less than 2 parts per million. No cracks, inclusions, or other imperfections were visible inside the crystal, which was optically clear. Laser ablation ICP-MS measurements on a fragment of this specimen showed that, despite some zoning visible by cathodoluminescence, the trace elements were homogeneous with concentrations, including Hf^{177}, mostly below the median trace element abundances of Mud Tank zircon as given in Gain et al. (2019). The sole exception was Nb^{93} with an average of 17.25(0.3) ppm Nb in our sample compared with 7.99 ppm Nb as a global average in Mud Tank zircons (Gain et al. 2019).

The RUS technique has been described in detail by Migliori and Sarrao (1997). The Cambridge equipment makes use of DRS Modulus II electronics for data collection at room temperature and Stanford electronics (Migliori and Maynard 2005) for data collection at high temperatures. Measurements at room temperature were performed with the crystal resting directly between two PZT piezoelectric transducers. For measurements at high temperatures the crystal was held lightly across a pair of opposite corners between the tips of a pair of horizontal alumina buffer rods which are inserted into a Netzsch resistance furnace (McKnight et al. 2008). The driving and detecting transducers were attached to the ends of the buffer rods, outside of the furnace. Temperature was measured with a thermocouple placed within a few millimeters of the sample. A further small adjustment of the measured temperature scale was made by calibration against the $\alpha-\beta$ transition in quartz which gives a clear and sharp minimum in elastic moduli at 846 K. The estimated accuracy of measured temperatures was considered to be better than ±2 K. High-temperature spectra were collected in an automated heating and cooling cycle with nominal temperature steps of 100 K up to ~1200 K. A settle time of 20 minutes was allowed for thermal equilibration of the sample before the data collection at each temperature.

Values of the six independent elastic constants for crystallographic point group 4/mmm at room temperature were determined by fitting to the resonance frequencies of 52 peaks between

0.3 and 1.5 MHz using the DRS software (Migliori and Sarrao 1997). Not all the same resonances could be detected in the spectra collected at high temperatures primarily due to attenuation of the signal by the buffer rods. As a consequence, the frequencies of between 41 and 49 resonance peaks were used for fitting of the high-temperature single-crystal elastic moduli. In order to obtain an internally consistent data set, the highest temperature data were fit first and the results were used as the starting values at the next temperature down. Changes in the shape of the crystal at each high temperature were calculated from a preliminary determination of the thermal expansion coefficient of zircon from literature data that is indistinguishable from the final *P*-*V*-*T* EoS described below. Root-mean-squared errors from the fitting were in the range of 0.31 to 0.37%. Values of the inverse mechanical quality factor, Q^{-1}, taken as $\Delta f/f$ where Δf was the peak width at half maximum height for a resonance peak with frequency $f \sim 1.0$ MHz, were close to 10^{-4} at each temperature. This low value is consistent with the sample being a high-quality single crystal. There was a slight dependence of final values of the elastic moduli on the starting values used in each case, signifying that the fitting surface has local minima. Uncertainties of the individual moduli were derived from the curvature of the solution surface in the vicinity of the minimum point (Migliori et al. 1990; Migliori and Maynard 2005) and therefore do not include uncertainties due to specimen shape, size, or orientation.

RESULTS

Compressional Study

The unit-cell volume of the Mud-Tank zircon was found to smoothly decrease as a function of pressure (Figure 1), up to a maximum hydrostatic pressure of 8.47(1) GPa. A fit of a third-order Birch-Murnaghan equation of state (EoS) with EosFit-GUI (Gonzalez-Platas et al. 2016) with full weights (Angel et al. 2014a) yielded the coefficients given in Table 2. Statistics improved marginally with a fit of a fourth-order Birch-Murnaghan EoS, with a slightly lower χ_w^2 and a minimal change in the values of the EoS parameters. *P*-*V* data points display significant curvature (Figure 1) and the data in the *f*-*F* plot exhibit a significantly positive slope implying that $K_{0T}' > 4$ and eliminating the possibility of a second-order Birch-Murnaghan EoS fitting the data. A third- or fourth-order Birch-Murnaghan EoS therefore provides the best statistical fit to our data.

The variation of the Mud-Tank zircon's unit-cell parameters with pressure (Figure 1) displays an anisotropic axial compressibility, with a/a_0 being more compressible than c/c_0. These results are consistent with axial compressibility data derived from the elastic tensor of zircon (Özkan et al. 1974). The axial data in the *f-F* plots displayed a linear trend, with a positive slope for *a* and a negative slope for *c*; therefore, these data were fit with third-order Birch-Murnaghan EoS to obtain the axial parameters given in Table 2.

RUS results

The elastic moduli measured before heating are reported in Table 3 together with the high-temperature results, along with the adiabatic Reuss bulk (K_S) and shear moduli (G_S) and the adiabatic linear moduli, M_{aS} and M_{cS}, for the *a*- and *c*-axes calculated from the individual tensor components. The estimated standard deviations (e.s.d.'s) associated with the bulk and linear moduli derived from the e.s.d.'s of the C_{ij} values are on the order of ~1%. The elastic moduli do not show any anomalous behavior that would indicate significant decomposition or a displacive phase transition of the crystal; the room-temperature values of the moduli at the end of the run are within the experimental uncertainties of those at the start, except for C_{66} which was slightly stiffer at the end. If this difference is real, it may indicate some slight change in crystallinity in the sample as a consequence of heating.

Our values of the individual shear moduli C_{44} and C_{66} at room temperature, and the value of the Reuss average shear modulus G_S, agree with those derived from ultrasonic wave velocity measurements of non-metamict zircon by Özkan et al. (1974). But our values of compressional moduli C_{11} and C_{33} are 2% higher, and C_{12} and C_{13} about 7% higher, than those previous measurements. This leads to a bulk modulus at room conditions (Figure 2) that is approximately 3.5% higher, although our measured temperature dependence dK_S/dT is in good agreement with the data of Özkan and Jamieson (1978) as re-evaluated by Özkan (2008). This difference cannot be due to radiation damage which softens the bulk modulus (Binvignat et al. 2018) because the diffraction peak widths of the sample used for the compression experiment indicate a very low degree, if any, of radiation damage in that sample. This suggests that the offset in bulk moduli values may be a systematic error in our data that arises from the fact that the resonances of a millimeter-sized sample primarily involve shearing motions and relatively little breathing motion

This is the peer-reviewed, final accepted version for American Mineralogist, published by the Mineralogical Society of America.
The published version is subject to change. Cite as Authors (Year) Title. American Mineralogist, in press.
DOI: https://doi.org/10.2138/am-2021-7731. http://www.minsocam.org/

so the shear elastic constants are constrained more tightly than those which contribute to the bulk modulus. The small misorientation errors and slight damage to the edges of the sample may also contribute to the offset in bulk moduli values.

P-V-T EoS

Pressure-volume data from the compressional study and the RUS data were combined with temperature-volume data reported in the literature to determine the *P-V-T* EoS of zircon. Only the *T–V* data in the range 100–1200 K were considered in the current analysis since the unit-cell parameters can be affected by the decomposition of zircon or a proposed displacive structural change at about 1200 K (e.g., Mursic et al. 1992). In order to allow for the different calibrations of diffractometers used to collect the published *T–V* data, each dataset was first scaled by the measured volume at room conditions to obtain V/V_0 (Figure **3**), and then recalculated as molar volumes by using $V_0 = 39.260$ cm^3/mol (Holland and Powell 2011). This means that published datasets without measurements at room conditions had to be excluded from fitting. Individual data points that are significant outliers from the general trends of the literature data, whether in volume or cell parameters (e.g., Subbarao and Gokhale 1968; Bayer 1972), were also excluded. All data used in fitting the EoS are listed in Table **4**. Fits were performed with EosFit7c (Angel et al. 2014a), using the methods of Milani et al. (2017) to fit the EoS to both volume and the adiabatic bulk moduli data simultaneously. When converted to molar volumes, the new *P-V* data implied a very slightly different value of V_0 than the value from Holland and Powell (2011). Rather than scaling these data in advance of the fitting, which would bias the final results and parameter values, we have implemented the refinement of dataset scale factors in EosFit7c, and separate scale factors were refined for the *V-T*, *P-V* datasets and the dataset of bulk moduli from the RUS measurements.

A thermal pressure EoS was employed to fit the data listed in Table **4**, in which the pressure at any V and T is considered as the sum of the reference pressure P_{ref} needed to reach a volume V at a reference temperature T_0, and the thermal pressure ΔP_{th} necessary to travel along an isochor to reach a final temperature T. The thermal pressure induced by heating along the isochor is given by the thermodynamic identity (e.g., Anderson 1995):

This is the peer-reviewed, final accepted version for American Mineralogist, published by the Mineralogical Society of America.
The published version is subject to change. Cite as Authors (Year) Title. American Mineralogist, in press.
DOI: https://doi.org/10.2138/am-2021-7731. http://www.minsocam.org/

$$\Delta P_{th} = \int_{T_0}^{T} (\alpha_V K_T)_V \, dT. \quad (1)$$

Different thermal-pressure EoS are distinguished by the method used to calculate ΔP_{th} through (1). The application of the Debye model in the MGD EoS is advantageous as it presents a simple technique to model ΔP_{th} using relatively few parameters and assumptions. The MGD EoS uses the Grüneisen relation to define the relationship between the elastic properties of a material and its heat capacity:

$$\alpha_V K_T = \frac{\gamma C_{vm}}{V_m}, \quad (2)$$

where C_{vm} is the molar heat capacity at constant volume, V_m is the molar volume, and γ is the dimensionless Grüneisen coefficient (e.g., Grüneisen 1912; Anderson 1995). It follows from (2) that ΔP_{th} can also be expressed in terms of γ and C_{vm}:

$$\Delta P_{th} = \int_{T_0}^{T} \left(\frac{\gamma C_{vm}}{V_m}\right)_V \partial T, \quad (3)$$

where T and T_0 are the final and initial reference temperature conditions. The MGD EoS uses the Debye model of the phonon density of states to define C_{vm} as:

$$C_{vm} = 9NR\left(\left(\frac{T}{\theta_D}\right)^3 \int_0^{\theta_D/T} \frac{x^4 e^x}{(e^x - 1)^2} \, dx\right), \quad (4)$$

where R is the gas constant, Θ_D is the Debye temperature, and N is the number of atoms in the formula unit. The quasi-harmonic approximation (QHA) assumes that γ is only a function of volume, allowing γ to be removed from the integral in (3). We can incorporate (4) into a simplified (3) to define the thermal pressure (ΔP_{th}):

$$\Delta P_{th} = \frac{3N\gamma}{V_m} R\left(TD\left(\frac{\theta_D}{T}\right) - T_0 D\left(\frac{\theta_D}{T_0}\right)\right), \quad (5)$$

where $D\left(\frac{\theta_D}{T}\right)$ is the Debye function (Debye 1912). The volume dependence of the Grüneisen coefficient γ consistent with the QHA is given by:

$$\gamma = \gamma_0 \left(\frac{V}{V_0}\right)^q, \quad (6)$$

This is the peer-reviewed, final accepted version for American Mineralogist, published by the Mineralogical Society of America.
The published version is subject to change. Cite as Authors (Year) Title. American Mineralogist, in press.
DOI: https://doi.org/10.2138/am-2021-7731. http://www.minsocam.org/

where q is the Anderson-Grüneisen parameter and γ_0 is the Grüneisen parameter at reference conditions (Anderson 1968). Lastly, the Debye temperature (Θ_D) is expressed as:

$$\theta_D = \theta_{D0}\, exp\left(\frac{\gamma_0 - \gamma}{q}\right), \quad (7)$$

where Θ_{D0} is the Debye temperature at reference conditions.

Because the thermal pressure from an MGD EoS involves the molar volume (e.g., Equation (3)), we kept this fixed at the literature value of 39.26 cm^3/mol (Holland and Powell 2011) and we refined the dataset scale factors. A full refinement of a Mie-Grüneisen-Debye thermal-pressure EoS with a third-order Birch-Murnaghan EoS was performed with full weights and yielded $\chi_w^2 = 0.70$. Refined EoS parameters from this fitting are reported in Table **5**. It is important to note that compressibility parameters from the *P-V-T* EoS agree with the EoS coefficients from *P-V* fitting within 1σ (see Table **2**). The scale factors (Table **5**) for the two volume datasets are close to unity and account for small differences in instrument calibrations and laboratory "room conditions".

The value of $K_{0S} = K_{0T}(1 + \alpha_0\gamma_0 T_0)$ calculated from our thermal-pressure EoS is 225.0(1.2) GPa, which agrees well with independent measurements at room conditions (Özkan et al. 1974; Özkan and Jamieson 1978). Note that the scale factor for the RUS data (Table **5**) means that our experimental values of K_S are consistently 3% higher than the calculated values from the EoS (Figure **2**). As discussed above, this may be attributed to the combination of lack of constraints on the compressional moduli by the RUS data from such a small sample and the effects of imperfections in the sample including misorientation errors of the sample faces, and the damage to corners and edges.

The value of K_{0T}' has been poorly constrained within the literature, with reported values ranging from 3.9 to 6.61 (Özkan and Jamieson 1978; Van Westrenen et al. 2004), while a re-analysis of all literature data together yields K_{0T}' = -0.56 (Zaffiro 2019). The value of K_{0T}' from our thermal-pressure EoS is 4.9(3), in the middle of this range and in good agreement with K_{0T}' = 4.71(4) from a recent series of DFT simulations (Stangarone et al. 2019). Additionally, the dK_S/dT value from our thermal-pressure EoS at 300 K and ambient pressure is -0.0156 GPa/K,

which is in good agreement with the numerically-calculated values of -0.0152 and -0.0164 GPa/K at 300 K and ambient pressure (Özkan 2008).

The isochoric heat capacity of an MGD EoS for zircon is given directly at any pressure or temperature for which we know the molar volume V_m, by Equation (4). The isobaric heat capacity C_p follows from:

$$C_p = C_v + TV_m\alpha^2K_T. \quad (8)$$

The C_p values from our EoS as a function of temperature are in reasonable agreement with the least-squares fitting of C_p derived from calorimetric zircon data (O'Neill 2006; Figure 4). This curve fits our calculated data closely but not exactly, probably because higher-frequency vibrational modes, including the Si-O stretching band, are not represented in the Debye model.

A C_p curve derived from DFT calculations of the calorimetric and electronic properties of zircon (Terki et al. 2005) also shows good agreement with the data in Figure 4. Additionally, Terki et al. (2005) calculated a Debye temperature Θ_D = 887 K at 0 K using a quasi-harmonic Debye model, which falls within 1σ of the calculated Debye temperature 849(38) K from our thermal-pressure EoS at 0 K. This is also remarkably similar to the Debye temperature Θ_D = 870 K extrapolated from a neutron-weighted phonon density of states map of a polycrystalline zircon (Nipko and Loong 1997; Chaplot et al. 2006). The rate of change with temperature of the Debye temperature of our MGD EoS is, however, about one-half that calculated by Terki et al. (2005), which may be a consequence of the different methods used to calculate the Debye temperature (as in McLellan 1980).

Cell parameter equations for *PT*

In EosFit, the parameters to describe the variation of the unit-cell parameters are obtained by fitting the cubes of the unit-cell parameters and treating them as volumes (Angel et al. 2014a). This yields linear moduli and thermal expansion coefficients that agree with independent determinations. However, it is not clear how to modify this approach so as to be able to treat the cell parameters as quantities equivalent to molar volumes that would be required to fit them with a linearized MGD EoS, nor what the refined parameters such as Debye temperature or γ_0 physically represent. Therefore we use an "isothermal type" of EoS (Angel et al. 2018) for describing the unit-cell parameter variation and, for internal consistency, we also report in Table

This is the peer-reviewed, final accepted version for American Mineralogist, published by the Mineralogical Society of America.
The published version is subject to change. Cite as Authors (Year) Title. American Mineralogist, in press.
DOI: https://doi.org/10.2138/am-2021-7731. http://www.minsocam.org/

278 **6** the corresponding parameters for this kind of EoS to describe the volume. In the absence of a
279 physical model for this type of EoS, unlike the MGD, there are more parameters, some of which
280 such as γ_0, q, and δ' are, either individually or collectively, not constrained by the data available.
281 The values of γ_0 and q have therefore been fixed to those refined for the MGD EoS, and δ' has
282 been given a value to reproduce the variation of K_{0T}' of the MGD EoS. Up to 5 GPa and 1200 K
283 this isothermal EoS gives volumes within 0.003%, bulk moduli within 0.1% and K_{0T}' within 0.02
284 of the values predicted by the refined MGD EoS.

285 In order to obtain parameters to describe the cell parameter variation in P and T (Table
286 **6**), we fixed the value of γ_{i0} for each axis to the value of γ_0 for the volume, multiplied by the ratio
287 $M_{i0}/3K_0$ (Milani et al. 2017), and the values of q, and δ' to those for the volume EoS. These
288 constraints are sufficient to allow refinement of the other EoS parameters to describe the a-axis
289 (Table **6**) but the c-axis is so stiff that the value of δ, which controls dK/dT, cannot be refined
290 and a value was chosen that reproduces the general trend of the data. These sets of EoS
291 parameters are internally consistent in that the more uncertain values for the properties of the c-
292 axis given by its own EoS, are in good agreement within 10^{-4} in strain and 0.5 GPa in modulus
293 with those calculated from the ratio V/a^2 over metamorphic ranges of P and T. The refined axial
294 moduli correspond to adiabatic values at room conditions of 573(3) and 1042(13) GPa,
295 respectively, for the a- and c-axes respectively, in reasonable agreement with the values from
296 ultrasonic wave velocity measurements of 580 and 1012 GPa (Özkan et al. 1974).
297

298 **IMPLICATIONS**

299 The combined fit to our new RUS and P-V data together with the data available in the
300 literature yields a MGD EoS (Table **5**) and isothermal-type EoS (Table **6**) that are in good
301 agreement with previous determinations of the elastic tensor of zircon (Özkan 2008) and its
302 variation with temperature (Özkan 2008). But all of these measurements are significantly stiffer
303 than the bulk modulus obtained from powder diffraction data by van Westrenen et al. (2004), for
304 reasons that cannot be determined from the available published information. In particular, the
305 new P-V data resolve the previous discrepancy between the wide range of values of K_{0T}' reported
306 in the literature, including a value of -0.56 from a global fit of the literature P-V data (Zaffiro

This is the peer-reviewed, final accepted version for American Mineralogist, published by the Mineralogical Society of America.
The published version is subject to change. Cite as Authors (Year) Title. American Mineralogist, in press.
DOI: https://doi.org/10.2138/am-2021-7731. http://www.minsocam.org/

2019), and provide a value of K_{0T}' that is in good agreement with the recent DFT simulation of zircon (Stangarone et al. 2019). Our data therefore confirm experimentally that the displacive transition to the high-pressure phase of zircon above 20 GPa (Stangarone et al. 2019; Mihailova et al. 2019) is not accompanied by significant elastic softening, at least up to 8.5 GPa. The EoS parameters are provided in .eos files that can be read by the EosFit suite of programs both as supplementary material to this paper, and as files for free download from www.rossangel.net.

Pyrope garnets are common hosts for zircon inclusions and have EoS parameters $\alpha_H = 2.54 \times 10^{-5}$ K^{-1} and $\beta_H = 1/K_{0T} = 0.0061$ GPa^{-1} at room conditions (Milani et al. 2017), with the subscript 'H' indicating here the host mineral. These parameters are significantly larger than those of zircon; thus for zircon inclusions in a garnet host $\alpha_H > \alpha_I$ and $\beta_H > \beta_I$. As a consequence, the isomekes (Rosenfeld and Chase 1961), which define lines of equal fractional volume change of the two phases, have steep positive slopes given by $\left(\frac{\partial P}{\partial T}\right)_{isomeke} = \frac{\alpha_I - \alpha_H}{\beta_I - \beta_H}$. Figure **5** shows that the isomekes of zircon in garnet calculated with both the MGD and isothermal EoS for zircon reported in this work are indistinguishable. The significance of the isomekes is that a zircon trapped in a garnet at any point along a single isomeke will exhibit the same final inclusion pressure, P_{inc}, measured when the garnet is at room conditions (e.g., Rosenfeld and Chase 1961; Angel et al. 2014b, 2017). These P_{inc} values are indicated on the isomekes shown in Figure **5**. It is clear from the spacing of the isomekes that P_{inc} of zircon in garnet is more sensitive to temperature rather than pressure, and thus zircon inclusions in garnets are better piezothermometers than piezobarometers.

Normally, soft inclusions in stiffer hosts (such as quartz in garnet) yield positive inclusion pressures P_{inc} at room conditions (e.g., Angel et al. 2014b), whereas stiff inclusions in softer hosts such as zircon in garnet might be expected to have either negative or zero P_{inc} at room conditions. However, Figure **5** shows that the considerable contrast between the thermal expansion coefficients of zircon and garnet (α_I and α_H) that results in steep isomekes also places room pressure and temperature conditions above the isomekes that run through metamorphic conditions. As a consequence, room conditions lie in the region where P_{inc} is greater than the external pressure (e.g., Ferrero and Angel 2018), resulting in positive residual pressures in zircon inclusions trapped under metamorphic conditions.

The new EoS has a significantly lower thermal expansion coefficient and bulk modulus than the Holland and Powell (2011) EoS for zircon, whereas the EoS that can be obtained by fitting (Zaffiro 2019) previously published data also exhibits a high bulk modulus similar to that of Holland and Powell (2011), but has a thermal expansion coefficient similar to the one determined here. The smaller β_I determined by Zaffiro (2019) results in isomekes steeper than those shown in Figure 5 while the larger α_I and smaller β_I from Holland and Powell (2011) give isomekes with significantly shallower slopes. The consequence is that using the EoS from Zaffiro (2019) for zircon leads to inferred entrapment pressures at 700°C that are roughly 0.3 GPa greater than those calculated with our new EoS, and those calculated with the EoS from Holland and Powell (2011) can be up to 0.8 GPa lower.

In this study we have also introduced the refinement of scaling of datasets during the fitting of EoS with the EosFit program. This allows different datasets, whether of volume or bulk moduli, to be used together without biasing the final results by scaling of the data prior to fitting. In particular, this can accommodate the small differences in volumes frequently found between datasets from diffraction data that arise from both the different calibrations of diffractometers and uncharacterized differences in laboratory temperatures, frequently simply reported as "room temperature". We have shown that this rescaling can also accommodate the differences in absolute values of the bulk moduli arising, for example in this study, from the necessity of using a sample that was half the ideal size required for RUS measurements. Such scaling could also accommodate the differences in bulk moduli of single crystal and polycrystalline specimens, allowing data from both types of elasticity measurements to be fitted together in a self-consistent manner. Lastly, we note that the reasonable agreement (Figure 4) between the heat capacity obtained from our EoS and from measurements (O'Neill 2006) suggests the possibility of refining EoS parameters not only to volume and bulk moduli data, but also simultaneously to experimentally-determined C_p data.

ACKNOWLEDGEMENTS

We thank John Valley for donating the sample of Mud-Tank zircon used in the compressional experiments. We also thank Raphael Nujl of the Bayerisches Geoinstitut for preparing the

365 sample for RUS measurements, Mattia Bonazzi and Antonio Langone for the chemical analysis
366 of the sample in Pavia, Jing Zhao for his assistance and advice with the high-pressure diffraction
367 measurements at Virginia Tech. We thank Herbert Kroll and Peter Schmid-Beurmann (Münster)
368 for discussions about fitting EoS and Mattia Gilio (Pavia) for test calculations of isomekes with
369 zircon. RUS facilities were established in Cambridge through grants from the Natural
370 Environment Research Council and the Engineering and Physical Sciences Research Council of
371 Great Britain to MAC (NE/B505738/1, NE/F17081/1, EP/I036079/1). This project was funded
372 from the European Research Council under the European Union's Horizon 2020 research and
373 innovation program grant agreement 714936 TRUE DEPTHS to Matteo Alvaro. Alix Ehlers and
374 Nancy Ross were funded by the U.S. Department of Energy grant DOE-SC0016448 and the
375 National Science Foundation grant NSF MRI-1726077.

376

377

REFERENCES

Anderson, O.L. (1968) Some remarks on the volume dependence of the Grüneisen parameter. Journal of Geophysical Research, 73, 5187-5194.

Anderson O.L. (1995) Equations of State of Solids for Geophysics and Ceramic Science, 432 p. Oxford University Press, Inc., U.K.

Angel, R.J., and Finger, L.W. (2011) SINGLE: a program to control single-crystal diffractometers. Journal of Applied Crystallography, 44, 247-251.

Angel R.J., Gonzalez-Platas J., and Alvaro, M. (2014a) EosFit7c and a Fortran module (library) for equation of state calculations. Zeitschrift für Kristallographie, 229, 405-419.

Angel, R.J., Mazzucchelli, M.L., Alvaro, M., Nimis, P., and Nestola, F. (2014b) Geobarometry from host–inclusion systems: the role of elastic relaxation. American Mineralogist, 99, 2146–2149.

Angel, R.J., Nimis, P., Mazzucchelli, M.L., Alvaro, M., and Nestola, F. (2015) How large are departures from lithostatic pressure? Constraints from host–inclusion elasticity. Journal of Metamorphic Geology, 33, 801-813.

Angel, R.J., Mazzucchelli, M.L., Alvaro, M., and Nestola, F. (2017) EosFit-Pinc: a simple GUI for host–inclusion elastic thermobarometry. American Mineralogist, 102, 1957–1960.

Angel, R.J., Alvaro, M., and Nestola, F. (2018) 40 years of mineral elasticity: a critical review and a new parameterisation of Equations of State for mantle olivines and diamond inclusions. Physics and Chemistry of Minerals, 45, 95-113.

Bayer, G. (1972) Thermal expansion of ABO_4-compounds with zircon-and scheelite structures. Journal of the Less Common Metals, 26, 255-262.

Binvignat, F.A.P., Malcherek, T., Angel, R.J., Paulmann, C., Schlüter, J., and Mihailova, B. (2018) Radiation-damaged zircon under high pressures. Physics and Chemistry of Minerals, 45, 981-993.

Chaplot, S.L., Mittal, R., Busetto, E., and Lausi, A. (2002) Thermal expansion in zircon and almandine: Synchrotron x-ray diffraction and lattice dynamical study. Physical Review B, 66, 064302.

Chaplot, S.L., Pintschovius, L., and Mittal, R. (2006) Phonon dispersion relation measurements on zircon, $ZrSiO_4$. Physica B: Condensed Matter, 385, 150-152.

Debye, P. (1912) Zur Theorie der spezifischen Wärmen. Annalen der Physik, 344, 789-839.

Fedo, C.M., Sircombe, K.N., and Rainbird, R.H. (2003) Detrital Zircon Analysis of the Sedimentary Record. Reviews in Mineralogy and Geochemistry, 53, 277–303.

Ferrero, S., and Angel, R.J. (2018) Micropetrology: Are inclusions grains of truth? Journal of Petrology, 59, 1671-1700.

Finch, R.J., and Hanchar, J.M. (2003) Structure and chemistry of zircon and zircon-group minerals. Reviews in Mineralogy and Geochemistry, 53, 1-25.

Gain, S. E., Gréau, Y., Henry, H., Belousova, E., Dainis, I., Griffin, W. L., and O'Reilly, S. Y. (2019) Mud Tank Zircon: Long-term evaluation of a reference material for U-Pb dating, Hf-isotope analysis and trace element analysis. Geostandards and Geoanalytical Research, 43, 339-354.

Gonzalez-Platas, J., Alvaro, M., Nestola, F., and Angel R.J. (2016) EosFit7-GUI: A new GUI tool for equation of state calculations, analyses, and teaching. Journal of Applied Crystallography, 49, 1377-1382.

Grüneisen, E. (1912) Theorie des festen Zustandes einatomiger Elemente. Annalen der Physik, 344, 257-306.

Hanchar, J.M., and Hoskin, P.W.O. (2003) Zircon. Reviews in Mineralogy and Geochemistry, 53, 27-62.

Hazen, R.M., and Finger, L.W. (1979) Crystal structure and compressibility of zircon at high pressure. American Mineralogist, 64, 196-201.

Holland, T.J.B., and Powell, R. (2011) An improved and extended internally consistent thermodynamic dataset for phases of petrological interest, involving a new equation of state for solids. Journal of Metamorphic Geology, 29, 333-383.

Jackson, S.E., Pearson, N.J., Griffin, W.L., and Belousova, E.A. (2004) The application of laser ablation-inductively coupled plasma-mass spectrometry to in situ U–Pb zircon geochronology. Chemical Geology, 211, 47-69.

King, H.E., and Finger, L.W. (1979) Diffracted beam crystal centering and its application to high-pressure crystallography. Journal of Applied Crystallography, 12, 374-378.

McKnight, R.E., Moxon, T., Buckley, A., Taylor, P.A., Darling, T.W., and Carpenter, M.A. (2008) Grain size dependence of elastic anomalies accompanying the α-β phase transition in polycrystalline quartz. Journal of Physics: Condensed Matter, 20, 075229.

McLellan, A.G., Ed. (1980) The Classical Thermodynamics of Deformable Materials, 165 p., Cambridge University Press, U.K.

Migliori, A., and Sarrao, J.L., Eds. (1997) Resonant ultrasound spectroscopy: applications to physics, material measurements and non-destructive evaluation, 201 p., Wiley, New York.

Migliori, A., and Maynard, J.D. (2005) Implementation of a modern resonant ultrasound spectroscopy system for the measurement of the elastic moduli of small solid specimens. Review of Scientific Instruments, 76, 121301.

Migliori, A., Visscher, W.M., Brown, S.E., Fisk, Z., Cheong, S.W., Alten, B., Ahrens, E.T., Kubat-Martin, K.A., Maynard, J.D., Huang, Y., and others (1990) Elastic constants and specific-heat measurements on single crystals of La_2CuO_4. Physical Review B, 41, 2098.

Mihailova, B., Waeselmann, N., Stangarone, C., Angel, R.J., Prencipe, M., and Alvaro, M. (2019) The pressure-induced phase transition(s) of $ZrSiO_4$: revised. Physics and Chemistry of Minerals, 46, 807-814.

Milani, S., Angel, R.J., Scandolo, L., Mazzucchelli, M.L., Ballaran, T.B., Klemme, S., Domeneghetti, M.C., Miletich, R., Schiedl, K.S., Derzsi,, M., and others (2017) Thermo-elastic behavior of grossular garnet at high pressures and temperatures. American Mineralogist, 102, 851-859.

Miletich, R., Allan, D.R, and Kuhs W.F. (2000) High-pressure single crystal techniques. In R.M. Hazen and R.T. Downs, Eds., High-Temperature and High-Pressure Crystal Chemistry. 41, 445–519. Reviews in Mineralogy and Geochemistry, Mineralogical Society of America, Chantilly, Virginia.

Mursic, Z., Vogt, T., and Frey, F. (1992) High-temperature neutron powder diffraction study of $ZrSiO_4$ up to 1900 K. Acta Crystallographica Section B: Structural Science, 48, 584-590.

Nipko, J.C., and Loong, C.K. (1997) Inelastic neutron scattering from zircon. Physica B: Condensed Matter, 241, 415-417.

O'Neill, H.S.C. (2006) Free energy of formation of zircon and hafnon. American Mineralogist, 91, 1134-1141.

Ono, S., Tange, Y., Katayama, I., and Kikegawa, T. (2004) Equations of state of ZrSiO4 phases in the upper mantle. American Mineralogist, 89, 185-188.

Özkan, H. (2008) Correlations of the temperature and pressure dependencies of the elastic constants of zircon. Journal of the European Ceramic Society, 28, 3091-3095.

Özkan, H., and Jamieson, J.C. (1978) Pressure dependence of the elastic constants of nonmetamict zircon. Physics and Chemistry of Minerals, 2, 215-224.

Özkan, H., Cartz, L., and Jamieson, J.C. (1974) Elastic constants of nonmetamict zirconium silicate. Journal of Applied Physics, 45, 556-562.

Rosenfeld, J.L., and Chase, A.B. (1961) Pressure and temperature of crystallization from elastic effects around solid inclusion minerals? American Journal of Science 259, 519–541.

Scheidl, K.S., Kurnosov, A., Trots, D.M., Boffa Ballaran, T., Angel, R.J., and Miletich, R. (2016) Extending the single-crystal quartz pressure gauge up to hydrostatic pressure of 19 GPa. Journal of Applied Crystallography, 49, 2129-2137.

Stangarone, C., Angel, R.J., Prencipe, M., Mihailova, B., and Alvaro, M. (2019) New insights into the zircon-reidite phase transition. American Mineralogist, 104, 830-837.

Subbarao, E.C., and Gokhale, K.V.G.K. (1968) Thermal expansion of zircon. Japanese Journal of Applied Physics, 7, 1126.

Terki, R., Bertrand, G., and Aourag, H. (2005) Full potential investigations of structural and electronic properties of $ZrSiO_4$. Microelectronic Engineering, 81, 514-523.

Van Westrenen, W., Frank, M.R., Hanchar, J.M., Fei, Y., Finch, R.J., and Zha, C.S. (2004) In situ determination of the compressibility of synthetic pure zircon ($ZrSiO_4$) and the onset of the zircon-reidite phase transition. American Mineralogist, 89, 197-203.

Woodhead, J. D., and Hergt, J. M. (2005) A preliminary appraisal of seven natural zircon reference materials for in situ Hf isotope determination. Geostandards and Geoanalytical Research, 29, 183-195.

Yuan, H.L., Gao, S., Dai, M.N., Zong, C.L., Günther, D., Fontaine, G.H., Liu, X.M., and Diwu, C. (2008) Simultaneous determinations of U–Pb age, Hf isotopes and trace element compositions of zircon by excimer laser-ablation quadrupole and multiple-collector ICP-MS. Chemical Geology, 247, 100-118.

Zaffiro, G. (2019) Constraints on the equations of state of rutile and zircon: implications for geothermobarometry. Doctoral dissertation, Università degli studi di Pavia, Pavia, Italy.

499 # TABLES

500 Table 1: Unit-cell volume and axial parameters of the Mud-Tank zircon as a function of pressure
501 collected in this study.

P (GPa)	*a* (Å)	*c* (Å)	*V* (Å^3)
0.000100(1)	6.60633(11)	5.98228(20)	261.088(12)
0.186(10)	6.60431(09)	5.98114(17)	260.879(10)
0.861(09)	6.59647(12)	5.97703(20)	260.081(12)
1.746(12)	6.58654(14)	5.97216(23)	259.087(14)
2.351(10)	6.57984(20)	5.96947(34)	258.444(21)
3.188(12)	6.57111(15)	5.96386(25)	257.516(15)
3.481(08)	6.56815(12)	5.96236(24)	257.220(14)
4.309(08)	6.55982(12)	5.95687(23)	256.331(14)
4.710(14)	6.55561(13)	5.95498(28)	255.921(16)
5.176(09)	6.55088(11)	5.95262(21)	255.451(13)
6.205(09)	6.54085(11)	5.94629(21)	254.398(12)
6.465(09)	6.53828(12)	5.94497(24)	254.143(14)
6.673(08)	6.53635(17)	5.94386(33)	253.945(19)
6.956(10)	6.53367(13)	5.94209(24)	253.661(14)
7.174(09)	6.53141(12)	5.94092(23)	253.435(13)
7.706(08)	6.52640(17)	5.93752(33)	252.902(19)
7.952(12)	6.52411(13)	5.93655(25)	252.683(15)
8.465(11)	6.51936(13)	5.93353(25)	252.187(14)
8.294(10)*	6.52100(15)	5.93455(29)	252.357(17)
5.737(08)*	6.54513(17)	5.94955(32)	254.871(18)
2.832(10)*	6.57486(12)	5.96620(22)	257.912(13)

502 *Data collected during decompression.

503

This is the peer-reviewed, final accepted version for American Mineralogist, published by the Mineralogical Society of America.
The published version is subject to change. Cite as Authors (Year) Title. American Mineralogist, in press.
DOI: https://doi.org/10.2138/am-2021-7731. http://www.minsocam.org/

504 Table 2: Equation of state volume and unit-cell parameters for the Mud-Tank zircon.

	EoS	V_0 (Å^3)/L_0 (Å)	K_{0T}/M_{0T} (GPa)	K_{0T}'/M_{0T}'	K_{0T}''/M_{0T}'' (GPa^{-1})	χ_w^2
Volume	BM3	261.08(1)	224.9(1.2)	4.76(30)	-0.0233*	0.25
Volume	BM4	261.09(1)	222.8(2.8)	6.2(1.8)	-0.41(50)	0.23
a-axis	BM3	6.60632(10)	572.2(3.0)	16.80(0.78)	-0.127*	0.51
c-axis	BM3	5.98224(13)	1039(13)	-0.8(2.9)	-0.159*	1.04

505 *Value implied.

Table 3: Adiabatic elastic moduli of zircon.

T (K)	C_{11}	C_{33}	C_{13}	C_{12}	C_{44}	C_{66}	K_S	M_{aS}	M_{cS}	G_S
293(3)	431.4 (2.9)	500.4 (4.5)	160 (4.3)	75.3 (3.1)	113.46 (6)	48.92 (2)	233.3	594.5	1083.8	98.5
428(3)	424.47 (3.99)	489.88 (7.15)	154.48 (6.21)	72.77 (4.01)	112.57 (10)	48.78 (2)	228.0	584.0	1040.3	97.8
512(3)	421.93 (4.01)	490.66 (7.02)	157.02 (6.12)	74.63 (4.04)	111.89 (10)	48.56 (2)	228.7	582.5	1064.7	97.1
607(3)	415.24 (3.57)	482.96 (5.84)	153.5 (5.40)	74.77 (3.81)	110.93 (9)	48.65 (2)	225.1	575.3	1035.6	96.6
711(3)	413.99 (2.24)	484.97 (3.78)	157.15 (3.44)	76.46 (2.45)	109.79 (5)	48.3 (1)	226.6	574.9	1069.9	95.7
823(3)	409.02 (3.89)	479 (6.90)	155.23 (5.98)	75.83 (3.97)	108.89 (10)	48.03 (3)	223.9	568.5	1055.4	94.9
939(3)	404.64 (1.94)	477.84 (4.16)	156.87 (3.2)	75.44 (1.98)	107.72 (4)	47.84 (1)	222.9	561.4	1083.2	94.0
1056(3)	397.8 (4.10)	469.61 (7.37)	152.95 (6.35)	73.94 (4.19)	106.56 (10)	47.5 (3)	218.7	551.8	1053.7	93.1
1172(3)	392.82 (3.97)	463.89 (7.10)	152.08 (6.08)	74.09 (4.02)	105.42 (9)	47.2 (3)	216.6	546.3	1046.6	92.1

All values are adiabatic, in GPa. Uncertainties from fitting of the resonance frequencies are given in parentheses. Uncertainties in bulk, shear and linear moduli are estimated to be 1%.

506

507

This is the peer-reviewed, final accepted version for American Mineralogist, published by the Mineralogical Society of America.
The published version is subject to change. Cite as Authors (Year) Title. American Mineralogist, in press.
DOI: https://doi.org/10.2138/am-2021-7731. http://www.minsocam.org/

508 Table 4: Sources of data used in *P-V-T* EoS calculations.

Source	Data Type	*P* max (GPa)	*T* range (K)	Ndata
This study	Single-crystal XRD	8.47	Ambient	21
This study	RUS to determine K_S	Ambient	293-1172	9
Chaplot et al. (2002)	Powder XRD	Ambient	100-280	15
Mursic et al. (1992)	Neutron powder diffraction	Ambient	500-1200	8

509 Note: Ndata is the number of data points used from each source.

510 Table 5: *P-V-T* EoS parameters and scale factors using a 3rd-order Birch-Murnaghan and Mie-
511 Grüneisen-Debye thermal-pressure EoS.

Compressibility				
EoS	**V_0 (cm^3/mol)**	**K_{0T} (GPa)**	**K_{0T}'**	**K_{0T}'' (GPa^{-1})**
BM3	39.2600	224.5(1.2)	4.9(3)	-0.025*
Thermal expansion				
EoS	**Θ_D (K)**	**Atoms/formula unit**	**γ_0**	**q**
MGD	849(38)	6**	0.868(15)	2.37(80)
Scale factors				
	***P-V* data**	***T-V* data**	**RUS data**	
	1.00154(4)	0.99983(3)	1.030(8)	

512 *Value implied.

513 **Fixed value.

514

This is the peer-reviewed, final accepted version for American Mineralogist, published by the Mineralogical Society of America.
The published version is subject to change. Cite as Authors (Year) Title. American Mineralogist, in press.
DOI: https://doi.org/10.2138/am-2021-7731. http://www.minsocam.org/

515 **Table 6:** Refined parameters for "isothermal-type" EoS to volume and cell parameters of zircon.

	V	***a***	***c***
K_{0T}/M_{i0T} (GPa)	224.4(1.2)	571(3)	1036(13)
K_{0T}'/M_{i0T}'	4.9(3)	17.1(8)	-0.1(2.0)
α_{V0}/α_{iV0} (K^{-1})	1.02(2) x 10^{-5}	0.26(1) x 10^{-5}	0.49(1) x10^{-5}
Θ_E (K)	642(25)	709(43)	566(30)
δ	6.5(8)	9.9(1.2)	3.8*
δ'	3*	3*	3*
γ_0	0.868*	0.736*	1.337*
q	2.37*	2.37*	2.37*

516 *Fixed value.

517

518

This is the peer-reviewed, final accepted version for American Mineralogist, published by the Mineralogical Society of America.
The published version is subject to change. Cite as Authors (Year) Title. American Mineralogist, in press.
DOI: https://doi.org/10.2138/am-2021-7731. http://www.minsocam.org/

519

FIGURES

Figure 1: Pressure variation of unit-cell volume (black), *a*-axis length (red), and *c*-axis length (blue). The line for *P*-*V* is the MGD thermal-pressure EoS determined in this study and the lines for *P*-*a* and *P*-*c* are the isothermal-type EoS normalized to 298 K. These EoS are indistinguishable from those obtained from BM3 EoS fits to the new *P* data alone.

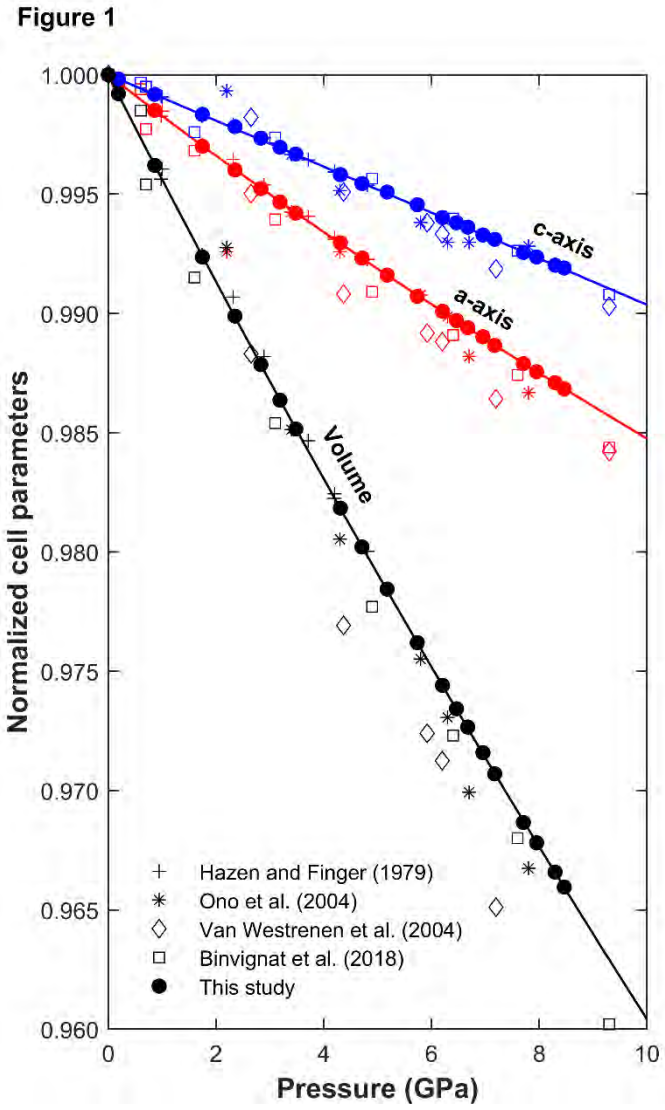

520

521

This is the peer-reviewed, final accepted version for American Mineralogist, published by the Mineralogical Society of America.
The published version is subject to change. Cite as Authors (Year) Title. American Mineralogist, in press.
DOI: https://doi.org/10.2138/am-2021-7731. http://www.minsocam.org/

522

Figure 2: Variation with temperature of experimental moduli data from the Mud-Tank zircon with the bulk modulus (lines) calculated from the MGD (Table 5) and linear moduli from isothermal-type EoS (Table 6). Dashed lines are moduli calculated without the scale factor and solid lines with the scale factor.

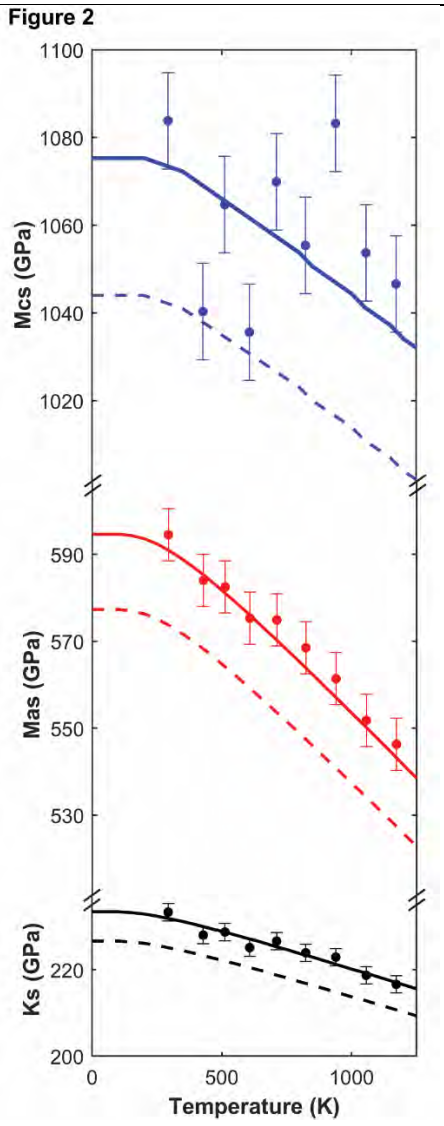

523

524

This is the peer-reviewed, final accepted version for American Mineralogist, published by the Mineralogical Society of America.
The published version is subject to change. Cite as Authors (Year) Title. American Mineralogist, in press.
DOI: https://doi.org/10.2138/am-2021-7731. http://www.minsocam.org/

525

Figure 3: The refined MGD thermal pressure EoS from this study (solid line) with the thermal pressure EoS from Holland and Powell (2011) (dashed line) normalized to $V_0 = 39.26$ cm^3/mol at 298 K plotted with T-V data. Data points with solid symbols were used in the fit of the EoS, while data with open symbols were excluded from the fit.

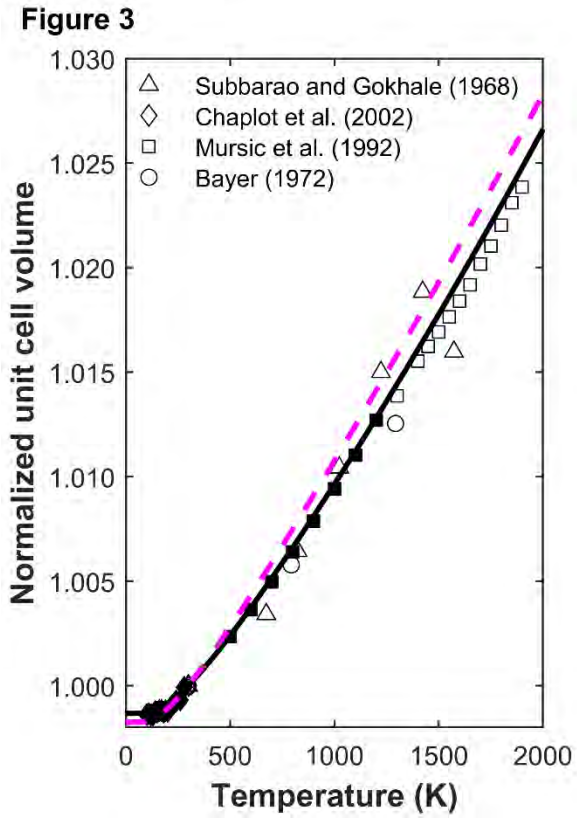

526

527

This is the peer-reviewed, final accepted version for American Mineralogist, published by the Mineralogical Society of America.
The published version is subject to change. Cite as Authors (Year) Title. American Mineralogist, in press.
DOI: https://doi.org/10.2138/am-2021-7731. http://www.minsocam.org/

Figure 4: Variation with temperature of the isobaric heat capacity of zircon (C_p). Dotted line: calculated C_p values from the MGD thermal-pressure EoS from this study; solid line: weighted least-squares fitting of zircon calorimetric data (O'Neill 2006)

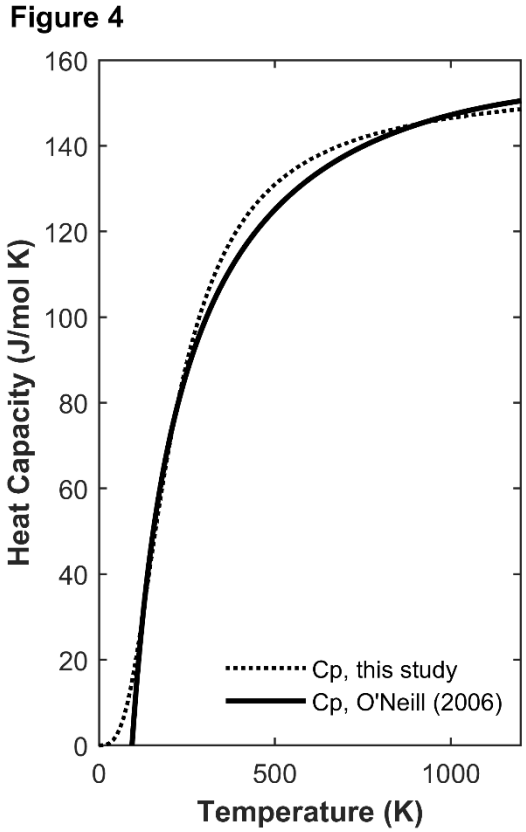

528

529

This is the peer-reviewed, final accepted version for American Mineralogist, published by the Mineralogical Society of America.
The published version is subject to change. Cite as Authors (Year) Title. American Mineralogist, in press.
DOI: https://doi.org/10.2138/am-2021-7731. http://www.minsocam.org/

Figure 5: Isomekes for zircon inclusions in pyrope for P_{inc} = 0-0.9 GPa. The solid black isomekes were calculated with the zircon MGD EoS (Table 5) and the blue dashed isomekes with the zircon BM3-isothermal EoS (Table 6). The parameters used for a BM3-MGD EoS for pyrope were K_{0T} = 169.9 GPa, K_{0T}' = 4.4, γ_0 = 1.19, q = 0, and Θ_D = 650 K.

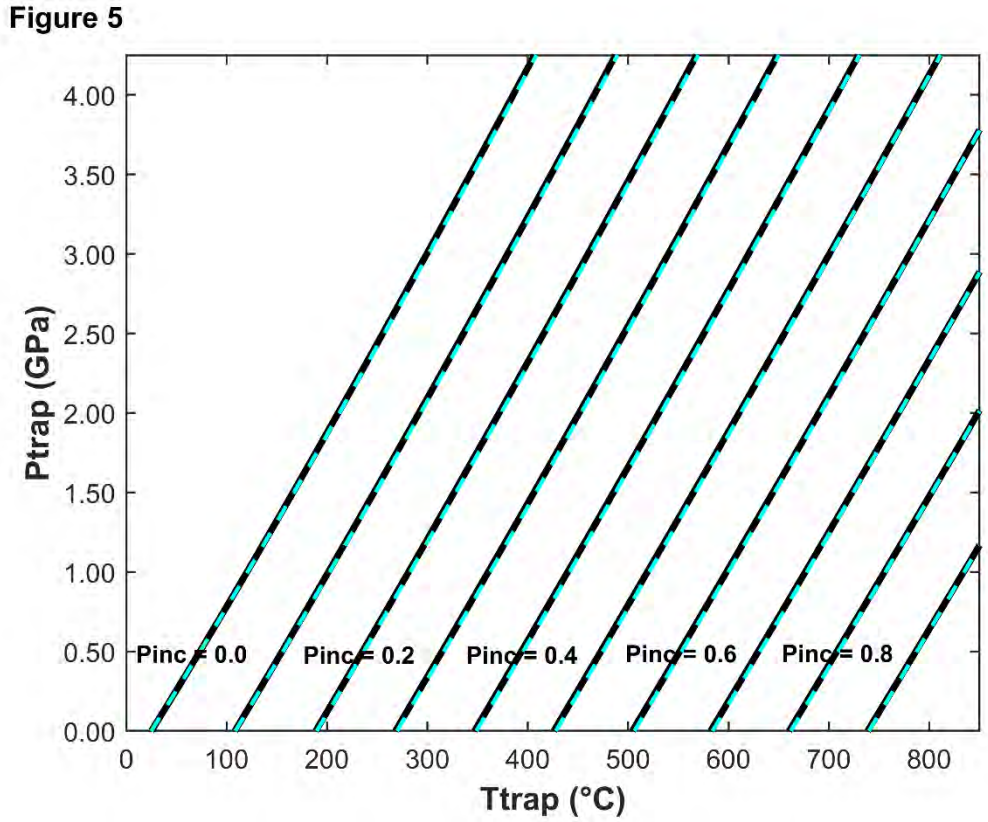

530